ISSN 1990-7931, Russian Journal of Physical Chemistry B, 2018, Vol. 12, No. 3, pp. 448–457. © Pleiades Publishing, Ltd., 2018.
Original Russian Text © V.Ya. Basevich, A.A. Belyaev, S.N. Medvedev, S.M. Frolov, F.S. Frolov, 2018, published in Khimicheskaya Fizika, 2018, Vol. 37, No. 6, pp. 44–54.

COMBUSTION, EXPLOSION, AND SHOCK WAVES

A Detailed Kinetic Mechanism of Multistage Oxidation and Combustion of Octanes

V. Ya. Basevich[a], A. A. Belyaev[a], S. N. Medvedev[a], S. M. Frolov[a, b, c, *], and F. S. Frolov[a, c]

[a] *Semenov Institute of Chemical Physics, Russian Academy of Sciences, Moscow, Russia*
[b] *National Research Nuclear University Moscow Engineering Physics Institute, Moscow, Russia*
[c] *Scientific Research Institute of System Development, Russian Academy of Sciences, Moscow, Russia*
**e-mail: smfrol@chph.ras.ru*

Received August 16, 2017

Abstract—This study has been focused on the construction of a generalized detailed kinetic mechanism of oxidation and combustion of isoheptane and isooctanes (2-methylhexane, 2-methylheptane, 2,2-dimethylhexane, and 2,2,4-trimethylpentane) to describe both high-temperature reactions and the low-temperature multistage process with separated stages of "cool," "blue," and "hot" flames. In accordance with the proposed mechanism, a numerical simulation of autoignition and flame propagation in homogeneous fuel–air mixtures and liquid droplet combustion has been conducted; the calculation results have been compared with the experimental data. Satisfactory qualitative and quantitative agreement of the calculation and experimental results has been obtained.

Keywords: alkanes, isoheptane, isooctanes, kinetic mechanisms, isobaric autoignition, compression-induced autoignition, multistage pattern, flame propagation, droplet combustion

DOI: 10.1134/S1990793118030223

INTRODUCTION

The author of [1] has generalized a large body of experimental data and introduced the concept of a multistage autoignition of hydrocarbons with separated stages of "cool," "blue," and "hot" flames. A multistage pattern is observed in experiments on the oxidation of many hydrocarbons, particularly isooctane, which is one of the reference motor fuels. It is of interest that, during the compression of isooctane, a separate region of existence of blue flames located outside the autoignition boundaries is observed [2]. Detailed kinetic mechanisms (DKMs) of oxidation and combustion of isomerized alkanes, such as C_7–C_{20} 2-methylalkanes [3] and isooctane (2,2,4-trimethylpentane) [4], have been proposed in the literature. However, none of the cited studies has proved that these mechanisms somehow describe the multistage autoignition with the three above stages. An exception is provided by [5]. The authors of that study, which addresses the phenomenology of autoignition of reference motor fuels—isooctane and *n*-heptane—refer to blue flame as "preignition" and propose a complex kinetic explanation to it (via reactions with aromatic structures), which cannot be applied to individual normal hydrocarbons and their isomers.

Previously, we have proposed a kinetic explanation for the occurrence of blue flame in the case of normal alkanes including cetane [6], isobutane [7], isopentane (2-methylbutane), isohexane (2-methylpentane) [8], isoheptane (2,2-dimethylpentane), and isooctane (2,2,4-trimethylpentane) [9]. The aim of this study is to construct an generalized DKM of oxidation and combustion of isoheptane and isooctanes (2-methylhexane, 2-methylheptane, 2,2-dimethylhexane, and 2,2,4-trimethylpentane) to describe both high-temperature and low-temperature reactions of multistage oxidation and combustion as adequately as reasonably possible. The choice of the above hydrocarbons is caused by an increase in the requirements for the accuracy of numerical simulations of oxidation and combustion of motor fuels in internal combustion engines (ICEs) [10].

CONSTRUCTION OF THE MECHANISM

As in [6–9], the most important reactions to describe the multistage oxidation and combustion of isooctanes were selected using the analogy technique. The construction of DKMs is based on a nonextensive approach, which assumes that low-temperature branching can be described by means of (1) a group of reactions with a single addition of an oxygen atom to the linear portion of the molecule and (2) a number of additional components limited to one of each of the main isomerized components that corresponds to each normal-structure component and represents the

Table 1. New reagents of the oxidation and combustion mechanism

No.	Component	Formula
1	Hydrocarbon 2-methylhexane	$CH_3CH(CH_3)C_4H_9$
2	Hydrocarbon radical	$CH_3CH(CH_3)C_4H_8$
3	Peroxy radical	$CH_3CH(CH_3)C_4H_8O_2$
4	Hydroperoxide	$CH_3CH(CH_3)C_4H_8O_2H$
5	Oxyradical	$CH_3CH(CH_3)C_4H_8O$
6	Aldehyde	$CH_3CH(CH_3)C_3H_6CHO$
7	Aldehyde radical	$CH_3CH(CH_3)C_3H_6CO$
8	Unsaturated hydrocarbon	$CH_3CH(CH_3)C_4H_7$
9	Unsaturated hydrocarbon radical	$CH_3CH(CH_3)C_4H_6$
10	Hydrocarbon 2-methylheptane	$CH_3CH(CH_3)C_5H_{11}$
11	Hydrocarbon radical	$CH_3CH(CH_3)C_5H_{10}$
12	Peroxy radical	$CH_3CH(CH_3)C_5H_{10}O_2$
13	Hydroperoxide	$CH_3CH(CH_3)C_5H_{10}O_2H$
14	Oxyradical	$CH_3CH(CH_3)C_5H_{10}O$
15	Aldehyde	$CH_3CH(CH_3)C_4H_8CHO$
16	Aldehyde radical	$CH_3CH(CH_3)C_4H_8CO$
17	Unsaturated hydrocarbon	$CH_3CH(CH_3)C_5H_9$
18	Unsaturated hydrocarbon radical	$CH_3CH(CH_3)C_5H_8$
19	Hydrocarbon 2,2-dimethylhexane	$CH_3C(CH_3)_2C_4H_9$
20	Hydrocarbon radical	$CH_3C(CH_3)_2C_4H_8$
21	Peroxy radical	$CH_3C(CH_3)_2C_4H_8O_2$
22	Hydroperoxide	$CH_3C(CH_3)_2C_4H_8O_2H$
23	Oxyradical	$CH_3C(CH_3)_2C_4H_8O$
24	Aldehyde	$CH_3C(CH_3)_2C_3H_6CHO$
25	Aldehyde radical	$CH_3C(CH_3)_2C_3H_6CO$
26	Unsaturated hydrocarbon	$CH_3C(CH_3)_2C_4H_7$
27	Unsaturated hydrocarbon radical	$CH_3C(CH_3)_2C_4H_6$

entire set of components having different structures, yet an identical gross formula.

Table 1 lists 27 additional components included in the new DKM of oxidation and combustion of isooctanes: 9 isomerized components for each of three hydrocarbons and their derivatives—isoheptane (2-methylhexane $CH_3CH(CH_3)C_4H_9$), 2-methylheptane (isooctane $CH_3CH(CH_3)C_5H_{11}$), and 2,2-dimethylhexane (isooctane $CH_3C(CH_3)_2C_4H_9$). The new DKM was constructed on the basis of analog mechanisms for normal octane C_8H_{18}, isobutane ($CH_3CH(CH_3)CH_3$), isopentane (2-methylbutane $CH_3CH(CH_3)C_2H_5$), isohexane (2-methylpentane $CH_3CH(CH_3)C_3H_7$), 2,2-dimethylpentane ($CH_3C(CH_3)_2C_3H_7$), and 2,2,4-trimethylpentane (isooctane $CH_3C(CH_3)_2CH_2CH(CH_3)CH_3$) [9] by adding reactions between these 27 additional components and all the components of the above analog mechanisms. As in [9], it was assumed that, for the oxidation of isomerized molecules, important elementary acts are only those that lead to deisomerization, i.e., to a decrease in the number of attached methyl groups to form stable intermediate isomerized and normal molecules. This means that the new DKM ignores elementary acts that lead to an increase in the linear portion of the molecule. In total, the new DKM includes 171 components and 2589 pairs of elementary reactions (each reaction occurs in the forward and reverse directions).

The lack of experimental data hinders the determination of the Arrhenius parameters—preexponential factor A and activation energy E—in the rate constants of the additional reactions. This problem can be solved as described in [7]: the missing parameters should be

determined from the available A and E values for reactions involving normal-structure components using the following two-parameter relationships:

$$A_{i(\mathrm{i})} = A_{i(\mathrm{n})} \exp[(\Delta S_{i(\mathrm{i})} - \Delta S_{i(\mathrm{n})})/R],$$

$$E_{i(\mathrm{i})} = E_{i(\mathrm{n})} - 0.25[\Delta H_{i(\mathrm{i})} - \Delta H_{i(\mathrm{n})}]$$

for exothermic reactions,

$$E_{i(\mathrm{i})} = E_{i(\mathrm{n})} + 0.75[\Delta H_{i(\mathrm{i})} - \Delta H_{i(\mathrm{n})}]$$

for endothermic reactions,

where $A_{i(\mathrm{i})}$ and $E_{i(\mathrm{i})}$ are the preexponential factor and the activation energy, respectively, in the expression for the rate of the ith reaction involving isomerized (subscript (i)) components; $A_{i(\mathrm{n})}$ and $E_{i(\mathrm{n})}$ are the preexponential factor and the activation energy, respectively, in the expression for the rate of the ith reaction involving only normal-structure (subscript (n)) components; $\Delta S_{i(\mathrm{i})}$ and $\Delta S_{i(\mathrm{n})}$ are the respective entropy changes in the reactions; $\Delta H_{i(\mathrm{i})}$ and $\Delta H_{i(\mathrm{n})}$ are the respective enthalpy changes in the reactions; T is the temperature; and R is the gas constant. It should be noted that, in accordance with [7], the derived Arrhenius parameters of some reactions involving isomerized components may require an adjustment because the critical phenomena—the occurrence of cool and blue flames in the case of multistage autoignition—take place only at a certain ratio of rates of the different elementary acts. It is clear that the adjustment is made in a range of values allowed by the theory, which do not exceed experimental errors.

The thermochemical parameters of the additional components included in the DKM—enthalpy of formation ΔH^0_{f298}, entropy S^0_{298}, and coefficients c_0, c_1, c_2, c_3, and c_4 in the formula for the specific heat at constant pressure $c_p = c_0 + c_1T/10^3 + c_2T^2/10^6 + c_3T^3/10^9 + c_4T^4/10^{12}$—are calculated on the basis of known recommendations and additivity rules [11].

VERIFICATION OF THE MECHANISM

Isobaric Autoignition of Gas Mixtures

The new DKM was verified by comparing the calculated and measured characteristics of the isobaric autoignition of isooctane–air mixtures at initial temperatures of T_0 = 600–1850 K and pressures of P = 10–20 atm; the composition of the reaction mixture ranged from fuel-lean to fuel-rich. Calculations were conducted using the KINET standard zero-dimensional kinetic program developed at Semenov Institute of Chemical Physics, Russian Academy of Sciences [12] and the CHEMKIN software [13].

Figure 1 shows typical calculated temperature–time dependences in the case of autoignition of a stoichiometric $CH_3CH(CH_3)C_5H_{11}$ isooctane–air mixture characteristic of high, moderate, and low initial temperatures. At high temperatures (above 1000 K),

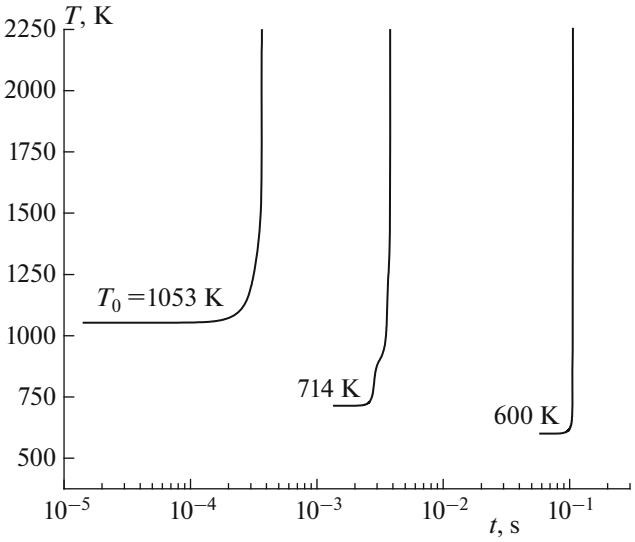

Fig. 1. Calculated temperature–time dependences in the case of autoignition of stoichiometric $CH_3CH(CH_3)C_5H_{11}$ isooctane–air mixtures at initial temperatures of T_0 = 1053, 714, and 600 K and a pressure of P = 20 atm.

autoignition occurs in a single stage. At a moderate temperature (714 K), autoignition looks like a two-stage process, although at 714 K and lower temperatures (600 K), autoignition is actually multistage, as evidenced from Fig. 2, which shows fragments of the temperature and kinetic curves obtained in calculations at a low temperature of T_0 = 600 K. In Fig. 2, the first stepwise temperature rise occurs at $t \sim 0.1052$ s; it corresponds to the occurrence of cool flame. The occurrence of blue flame (second stepwise temperature rise) and hot flame (third rise) is observed after a time interval of ~0.4 ms and at $t \sim 0.1058$ s, respectively. It is the sequential occurrence of cool, blue, and hot flames that is the manifestation of the multistage pattern of autoignition. An acceleration of the reaction in cool flame is a consequence of branching induced by the decomposition of isomerized alkyl hydroperoxide $CH_3CH(CH_3)C_5H_8O_2H$ to form hydroxyl and oxyradical. The occurrence of blue flame is attributed to branching caused by the decomposition of hydrogen peroxide H_2O_2, as evidenced by the behavior of the kinetic curves for the above peroxides and two peaks in the kinetic curve for hydroxyl. It should be emphasized that, in the experiment, owing to possible spatial inhomogeneities of the temperature field, the separation of stages according to the curves of the averaged parameters is not always so pronounced; however, in fact, it is locally implemented.

As a case in point, Fig. 3 shows comparison of calculated (curve) and measured (symbols [3]) autoignition delays for a stoichiometric $CH_3CH(CH_3)C_5H_{11}$ isooctane–air mixture at different initial temperatures and a pressure of 20 atm; Fig. 4 shows comparison of calculated (curves) and measured (symbols [3]) con-

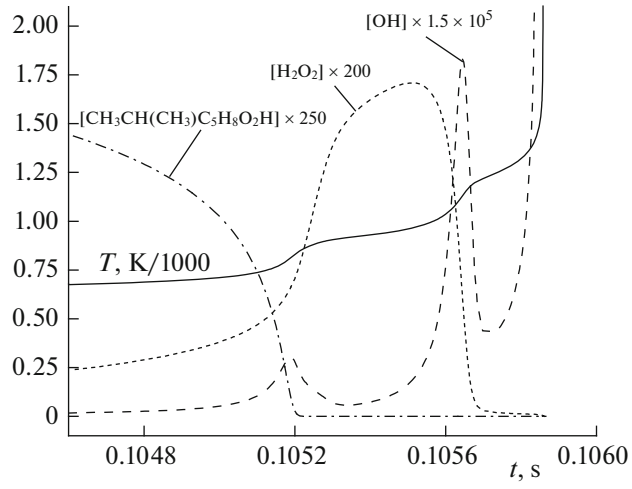

Fig. 2. Calculated time dependences of temperature T and concentrations of isomerized alkyl hydroperoxide $CH_3CH(CH_3)C_5H_8O_2H$, hydrogen peroxide H_2O_2, and hydroxyl OH in the case of autoignition of a stoichiometric $CH_3CH(CH_3)C_5H_{11}$ isooctane–air mixture at an initial temperature of $T_0 = 600$ K and a pressure of $P = 20$ atm.

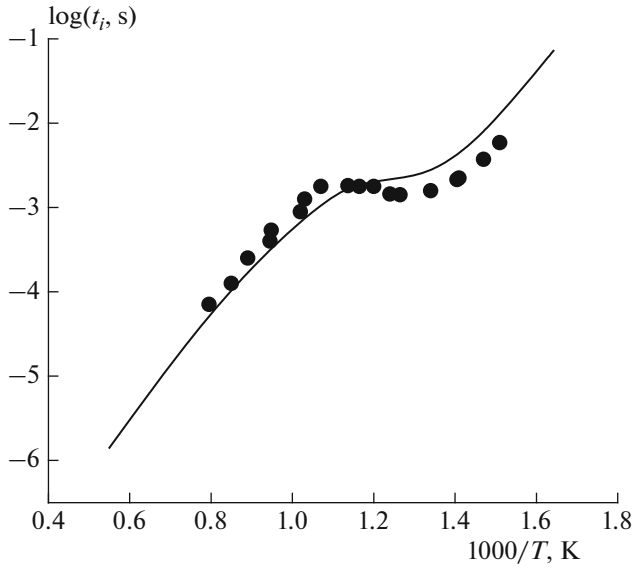

Fig. 3. Comparison of calculated (curve) and measured (symbols [3]) temperature dependences of autoignition delays for stoichiometric $CH_3CH(CH_3)C_5H_{11}$ isooctane–air mixtures at a pressure of $P = 20$ atm.

centrations of reaction products during the autoignition of isooctane $CH_3CH(CH_3)C_5H_{11}$ in a jet-stirred reactor at a pressure of 10 atm and a residence time of 0.7 s. Satisfactory agreement between the calculated and measured data is obtained.

Laminar Flame Propagation

The new DKM was additionally verified by comparing the calculated (curve) and measured (symbols [3]) dependences of laminar flame propagation velocity u_n on fuel–air equivalence ratio Φ for $CH_3CH(CH_3)C_5H_{11}$ isooctane–air mixtures at atmospheric pressure and an initial temperature of $T_0 = 353$ K (Fig. 5). The structure and velocity of one-dimensional laminar flame were calculated as described in [14].

Compression-Induced Autoignition under Conditions of an ICE

Compression-induced autoignition of isooctane and other hydrocarbons under conditions of an ICE was studied by a number of authors [2, 15, 16] as far back as the early 1950s. It was found [2] that, under these conditions, the region of autoignition in the compression ratio–air-to-fuel equivalence ratio plane (diagram in the right-hand side of Fig. 6) is immediately adjacent to the regions of preignition glow of blue and cool flames. In these regions, a partial reaction of the substance—a decrease in the fuel and oxygen concentrations, an increase in the pressure and temperature, and the formation of a certain amount of intermediate and final reaction products—is observed. Cool flame and blue flame glow is induced by electron-excited formaldehyde H_2CO^* and electron-excited formyl HCO^*, respectively [1, 17].

As noted above and in [6–9, 17], a simulation of the autoignition of hydrocarbons using DKMs shows that cool flame is initiated by the decomposition of alkyl hydroperoxide to form a highly reactive radical—hydroxyl OH; blue flame is initiated by a similar decomposition of hydrogen peroxide H_2O_2, which also leads to the formation of OH. For hydrocarbons, starting with ethane, these stages can be sequentially separated. It is of interest to reveal how the new DKM agrees with the known experimental data on the stages of compression-induced autoignition.

The kinetic identification of stages of low-temperature oxidation and autoignition of isooctane (2,2,4-trimethylpentane $CH_3C(CH_3)_2CH_2CH(CH_3)CH_3$) in air under piston compression is given below. The chemical kinetic processes that occur during the compression of a gas volume by a moving piston were calculated using the CHEMKIN-PRO Release 15083 computational program [13]. It was assumed that the ICE cylinder walls are adiabatic and that the neglect of heat transfer in a fast compression process cannot cause a significant qualitative change in the calculation results.

Figure 6 shows data of calculation (on the left) and experiment [2] (diagram on the right). In the calculated graphs constructed for different compression ratios ε, along the abscissa axis, time in terms of crank angle (CA) θ (in CA degrees (CAD)) is plotted and the piston top position (top dead center (TDC), 0° CAD) is marked; along the ordinate axis, pressure P in atm (curve *1*), temperature T in K (*2*), and the volume fractions of hydroxyl OH (*3*), isooctyl hydroperoxide

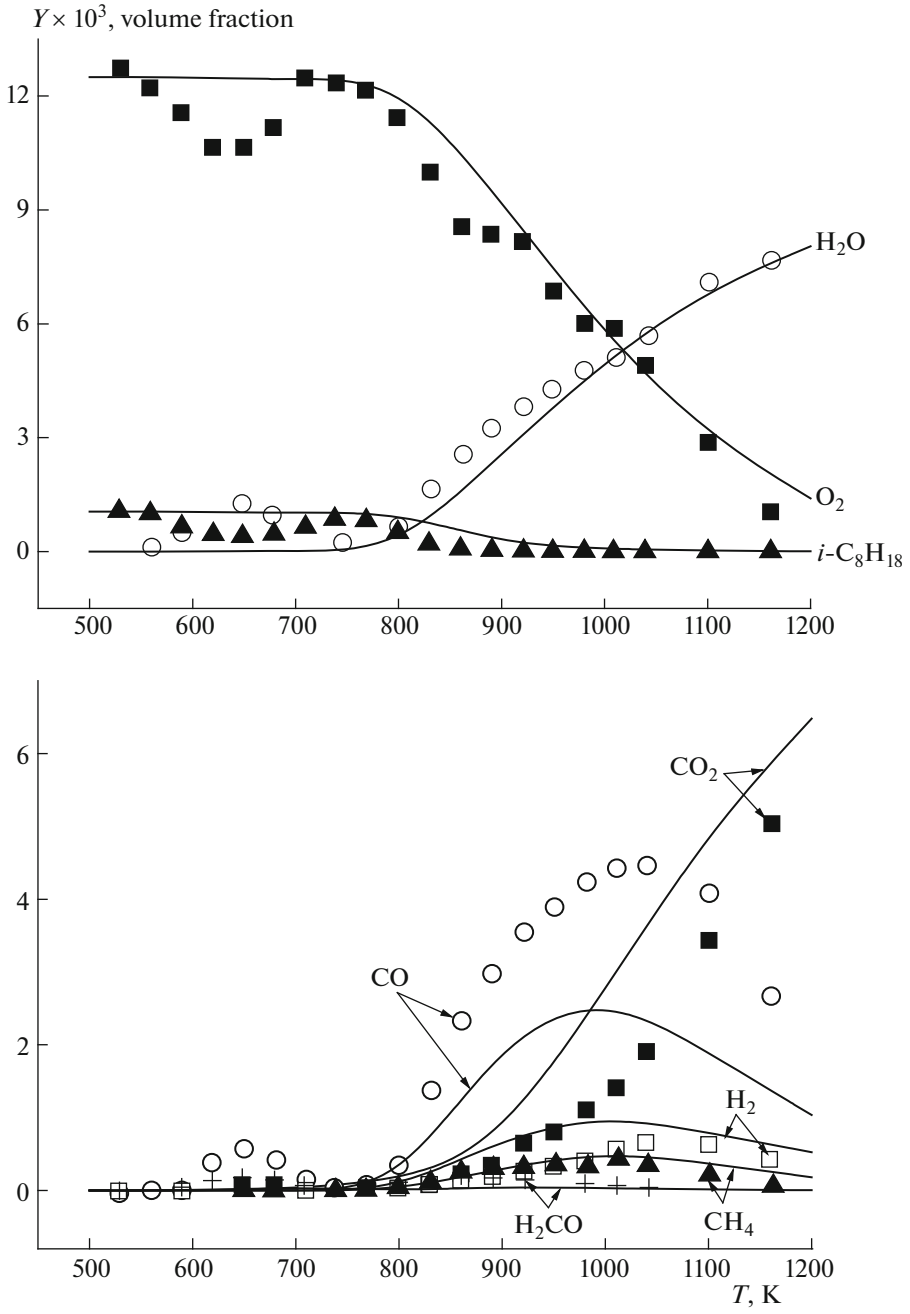

Fig. 4. Comparison of calculated (curves) and measured (symbols [3]) dependences of concentrations of the starting materials (i-C_8H_{18} and O_2) and the reaction products (H_2O, CO_2, CO, H_2, CH_4, CH_2O) in the case of autoignition of a stoichiometric $CH_3CH(CH_3)C_5H_{11}$ isooctane–air mixture in a jet-stirred reactor at a pressure of $P = 10$ atm and a residence time of 0.7 s.

$CH_3C(CH_3)_2CH_2CH(CH_3)CO_2H$ (*4*), and hydrogen peroxide H_2O_2 (*5*) are plotted. All calculations were conducted for a mixture with an air-to-fuel equivalence ratio of $\alpha = 1.5$ ($\Phi = 0.667$). For this mixture, a distinct separation of the boundaries of single cool flames and "double" cool, blue, and hot flames was observed in the experiment. All other calculation conditions were the same as in the experiment ($T_0 = 343$ K, $P_0 = 1$ atm, and an ICE shaft speed of $n = 1500$ rpm).

At $\varepsilon \le 12$, there are hardly any signs of the occurrence of a reaction in the calculation. Thus, at $\varepsilon = 12$, the pressure and temperature curves are almost symmetrical with respect to the axis showing the TDC position. In the experiment, this behavior of a combustible mixture with $\alpha = 1.5$ corresponds to $\varepsilon \approx 9$.

At $\varepsilon = 13$, in the calculated curves of pressure and temperature at $\theta \approx 7°$ CAD, the beginning of an increase corresponding to the heat release from a sin-

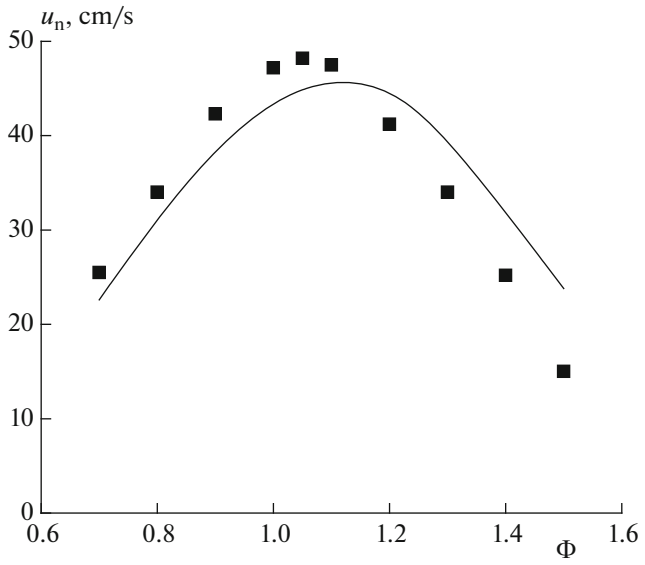

Fig. 5. Dependence of laminar flame propagation velocity u_n on composition Φ for $CH_3CH(CH_3)C_5H_{11}$ isooctane–air mixtures at atmospheric pressure and an initial temperature of $T_0 = 353$ K. The symbols stand for the experimental data [3]; the curve denotes the calculation.

gle cool flame is observed. In fact, the volume fraction of OH achieves a maximum value at θ ≈ 9° CAD, i.e., exactly at the maximum decomposition rate of isooctyl hydroperoxide. The volume fraction of H_2O_2 only increases. The occurrence of a single cool flame in a combustible mixture with α = 1.5 corresponds to an experimental value of ε ≈ 9–15.

According to the authors of [2], at higher values of compression ratio ε, double cool flames were observed in the experiment. We believe that, in fact, separated cool and blue flames, rather than the sequential occurrence of two cool flames, were observed in experiment [2]. In other words, a multistage autoignition characteristic of low-temperature oxidation of hydrocarbons took place. It is known [1] that, under laboratory conditions, periodic (or multiple) cool flames occur only at a negligible reaction depth provided that the gas is severely cooled by the vessel walls: only these conditions provide the reinitiation of a cool-flame reaction. These conditions are not implemented in ICEs.

According to the double peak of the volume fraction of OH arising during the expansion of the gas volume after the TDC, separate cool and blue flames are observed in the calculation starting with ε = 13.5. At the same time, the second peak is hardly visible in the pressure and temperature curves. The first (large) peak in the OH curve corresponds to the maximum decomposition rate of isooctyl hydroperoxide at θ ≈ 6° CAD; the formation of the second (small) peak begins at θ ≈ 7°–8° CAD; it is completely formed at θ ≈ 14° CAD, while isooctyl hydroperoxide still undergoes decomposition. Although hydrogen peroxide only accumulates under these conditions, the decomposition of H_2O_2 occurs already at a significant rate.

At ε = 13.75, a distinct separation of cool and blue flames is observed in the calculation. In this case, a double peak of OH is also observed; however, the volume fraction of OH is considerably higher than that at ε = 13.5. As before, the first peak corresponds to the decomposition of isooctyl hydroperoxide; the maximum decomposition rate is achieved at θ ≈ 4.2° CAD. The second peak, which alhas a larger amplitude, corresponds to the decomposition of accumulated hydrogen peroxide at θ ≈ 20° CAD, when the decomposition rate of H_2O_2 is maximal. In this case, the pressure and temperature are higher than the values in the previous calculations; however, the order of magnitude is the same (scale factor is preserved). Hot autoignition does not occur under these conditions.

With an increase in the compression ratio, the intensity of the blue flame glow increases and surpasses the weak glow of the cool flame. Under these conditions, the overall glow looks like a purely blue flame glow. Apparently, it is this feature that made the authors of [2] designate the lower blurred boundary of the blue flame region with a dashed line. The occurrence of double cool flames (actually, separated cool and blue flames) and purely blue flames in a combustible mixture with α = 1.5 in the experiment corresponds to values of ε ≈ 15–17 and 17–19.5, respectively.

Finally, at ε = 14, hot autoignition is observed in the calculation. The amplitude of the pressure and temperature peaks increases twofold; the peak of the volume fraction of hydroxyl increases by a few orders of magnitude (peak extends beyond the plot). The occurrence of hot autoignition in a combustible mixture with α = 1.5 in the experiment corresponds to values of ε > 19.5.

Table 2 shows results of an additional comparison of the results of calculations and experiments at different final compression temperatures T_{comp} (temperature at the TDC) corresponding to the selected values of compression ratio ε. In general, comparison of the calculation results with the experimental data suggests that the calculations are qualitatively consistent with the experimental data and make it possible to identify the observed effects.

Octane Droplet Combustion under Microgravity Conditions

A new—previously unobserved—phenomenon was reported by the authors of [18–20] in the cited and later studies. This phenomenon is the radiative extinction of a spherical hot flame around single droplets of individual hydrocarbon combustibles (methanol and *n*-heptane) and their subsequent low-temperature "cool-flame" combustion (in the terminology of [18–

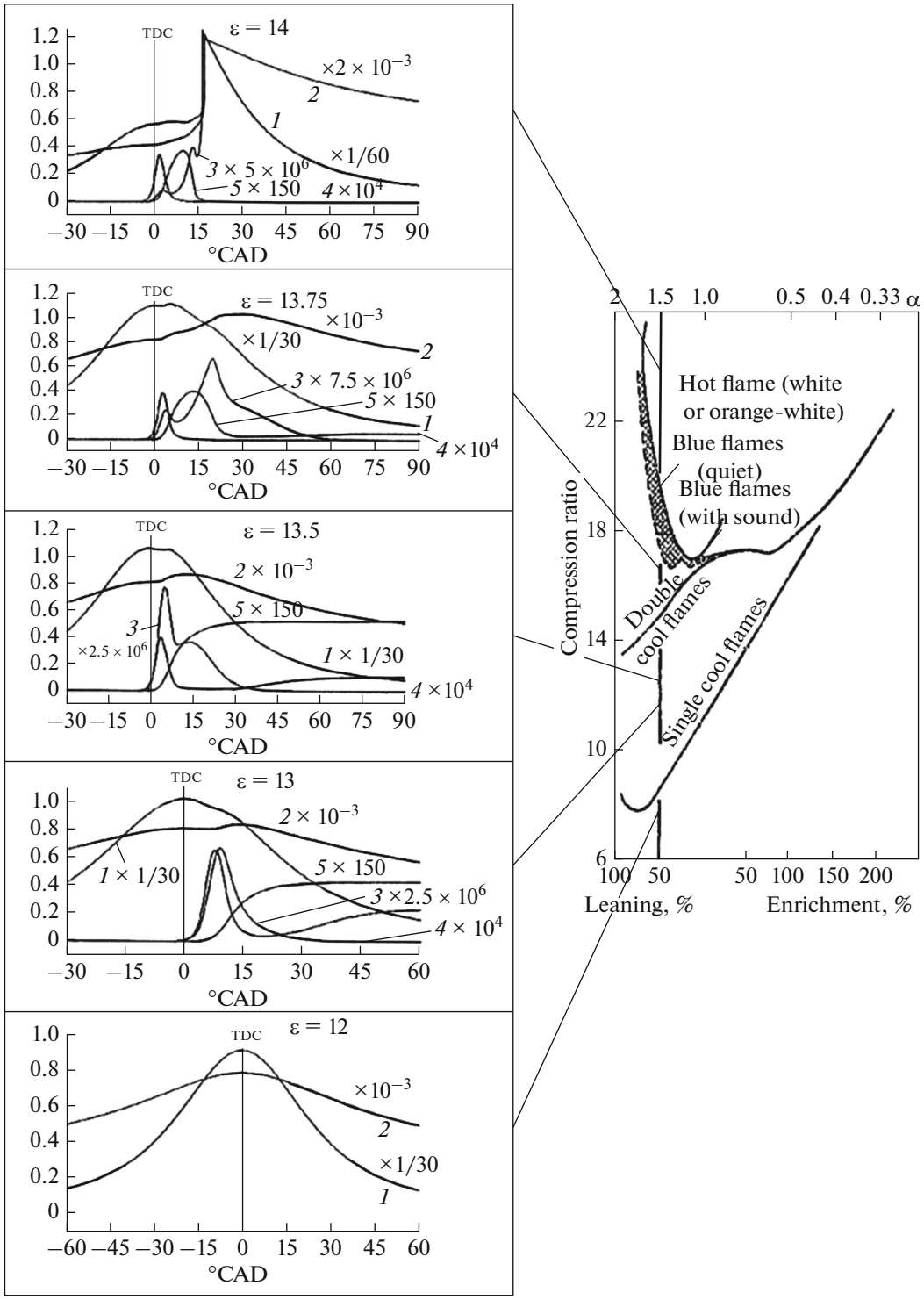

Fig. 6. On the right: boundaries of single cool flames and double cool, blue, and hot flames in the case of compression-induced autoignition of isooctane–air mixtures in an ICE at an initial temperature of $T_0 = 343$ K, an initial pressure of $P_0 = 1$ atm, and a shaft speed of $n = 1500$ rpm [2]. On the left: calculated dependences of (*1*) pressure P, (*2*) temperature T, and volume fractions of (*3*) hydroxyl OH, (*4*) isooctyl hydroperoxide $CH_3C(CH_3)_2CH_2CH(CH_3)CH_2O_2H$, and (*5*) hydrogen peroxide H_2O_2 on CA for an isooctane–air mixture with an excess air factor of $\alpha = 1.5$.

20]) under microgravity conditions aboard the International Space Station. Computational studies of this phenomenon were reported in the cited works. Sometimes, this low-temperature combustion of droplets without visible flames, i.e., flameless combustion, was accompanied by multiple hot flame flares.

Table 2. Calculated values of compression ratio ε and final compression temperature T_{comp} at T_0 = 343 K, P_0 = 1 atm, n = 1500 rpm, and α = 1.5

Reaction	ε	T_{comp}, K	Experimental range of T_{comp}, K [2]*
No visible reaction	12	<786	<703
Single cool flame	13	808	703–838
Double cool flames	13.5	816	838–882
Blue flame	13.75	820	882–914
Hot flame	14	>826	>914

*Approximate estimate according to compression ratio.

The authors of [21], in terms of a mathematical model of droplet combustion [22] supplemented with allowance for the radiation of soot and a DKM of oxidation and combustion of *n*-heptane [23] supplemented by a semiempirical soot formation mechanism [24], reproduced all the main features of the discovered phenomenon and predicted the existence of new modes of flameless combustion of droplets. Similar results were obtained for *n*-dodecane droplets in [25]. The calculations showed that, after the radiative extinction of hot flame, the droplet can continue to evaporate owing to the exothermic low-temperature oxidation of fuel vapors with multiple flashes of blue (rather than cool) flame at a characteristic temperature of 980–1000 K. A detailed analysis of the calculation results shows that regular temperature bursts are attributed to the thermal decomposition of hydrogen peroxide, i.e., branching leading to the formation of hydroxyl radicals.

To further verify the new DKM in terms of the droplet combustion model [21], the effect of fuel isomerization on the combustion of a droplet with an initial diameter of D_0 = 2.8 mm in air under microgravity conditions was studied. This task is one of the tasks of the joint Roscosmos–NASA space experiment named Cool Flames Investigation (in Russian, Zarevo), which was launched on board of the International Space Station in 2017. The air temperature and pressure selected for the calculations were 293 K and 1 atm, respectively. Thus, for droplets of four studied liquid octanes, essentially identical initial conditions were used in the calculations. Ignition with a heated wire or an electric discharge, which is used in space experiments, was simulated in the calculations by modeling a high-temperature spherical layer of width L leading to the occurrence of a hot flame around the droplet. Further, owing to the radiative extinction of the hot flame, the temperature of the gas around the droplet decreased; however, the droplet continued to vigorously evaporate owing to ongoing low-temperature exothermic reactions in the vicinity of the droplet.

Figure 7 shows comparison of the calculated time dependences of maximum gas temperature T_{max} around droplets of the different octanes. It is evident that, after the radiative extinction of the hot flame (initial temperature drop), the combustion of droplets of all the studied octanes continues; the maximum gas temperature around the droplet does not decrease below ~1100 K within a certain time t_b (see Fig. 7c). The droplet combustion is accompanied by temperature bursts, which correspond to flashes of blue and hot flames. The amplitude of these bursts and the duration of t_b are maximal for the *n*-octane droplet (Fig. 7a). With an increase in the degree of branching of the octane molecule (sequential transition from *n*-octane to 2-methylheptane, 2,2-methylhexane, and 2,2,4-trimethylpentane), the amplitude of the temperature bursts and the duration of t_b decrease and the maximum gas temperature around the droplet decreases (to 800 and 700 K in Figs. 7c and 7d, respectively). It was found that the temperature dependences derived for droplet combustion exhibit the same qualitative behavior as that of analogous dependences obtained for autoignition of homogeneous fuel–air mixtures. It is known that, in the low-temperature region, the oxidation and combustion rates of homogeneous mixtures of normal and isomerized alkane hydrocarbons with air differ from each other; the rates are lower for combustibles with branched molecules. It is evident from Fig. 7 that the oxidation and combustion rates for liquid droplets also decrease with increasing degree of branching of the molecule upon switching from *n*-octane to the reference isooctane (2,2,4-trimethylpentane).

CONCLUSIONS

A generalized DKM of the oxidation and combustion of octanes has been proposed. The mechanism includes the main processes that determine the reaction rate and the formation of the main intermediate and end products and has the status of an ab initio DKM because all the elementary reactions have a kinetic substantiation.

The most important distinctive feature of the proposed DKM is the manifestation of a multistage pattern in the form of occurrence of cool and blue flames in the case of the low-temperature autoignition of

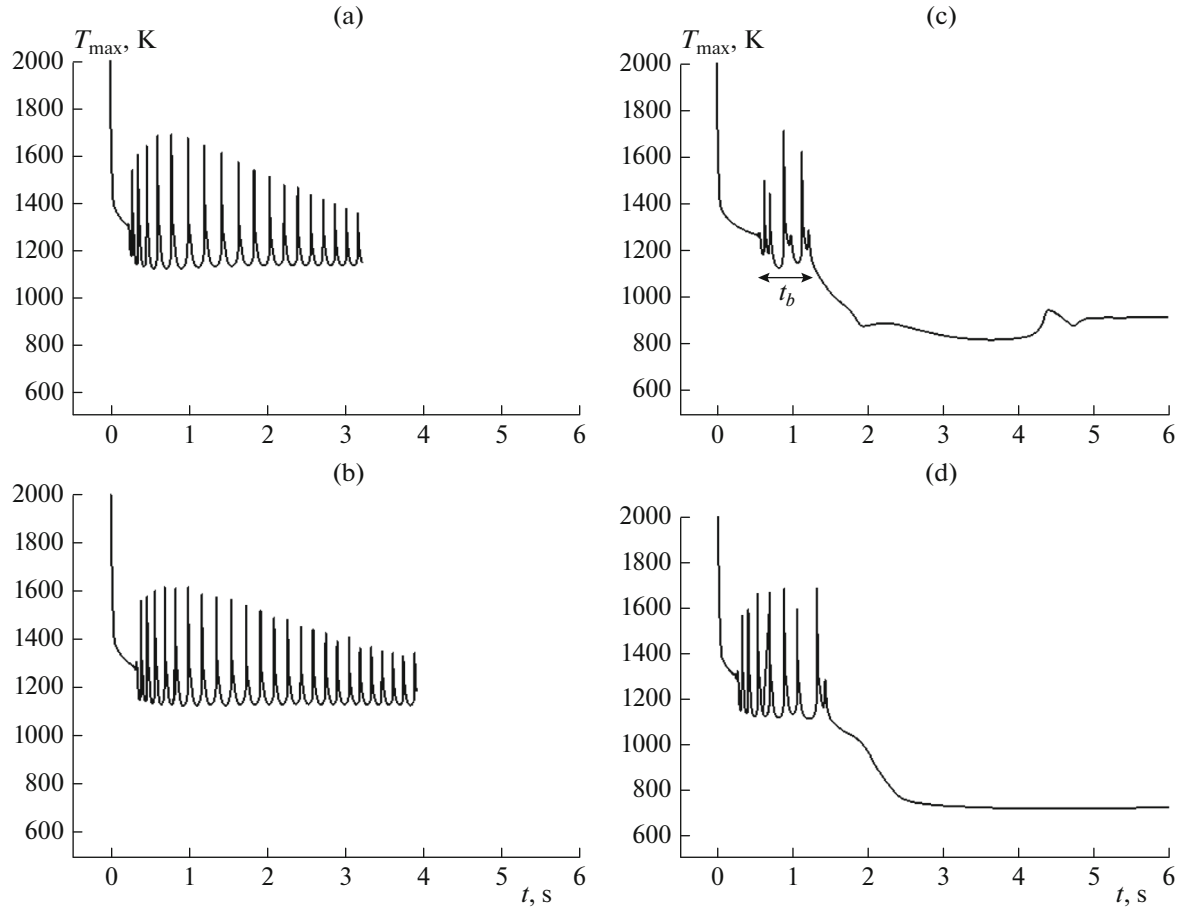

Fig. 7. Calculated dependences of maximum gas temperature T_{max} in the vicinity of droplets during combustion in air under microgravity conditions for four octanes: (a) *n*-octane, (b) 2-methylheptane, (c) 2,2-methylhexane, and (d) 2,2,4-trimethylpentane at a pressure of $P = 0.1$ MPa, an initial droplet diameter of $D_0 = 2.8$ mm, and an ignition layer thickness of $L = 0.525$ cm.

octanes. Calculations for the autoignition and combustion of homogeneous mixtures of various octanes with air in a wide range of initial conditions and the combustion of liquid octane droplets under microgravity have been conducted. The calculation results have been compared with the experimental data.

A file with the kinetic mechanism data and the respective thermodynamic data will be posted on the website www.combex.ru.

ACKNOWLEDGMENTS

This work was supported by the Russian Science Foundation (project no. 14-13-00082P) and performed within the frameworks of the Zarevo space experiment.

REFERENCES

1. A. S. Sokolik, *Self-Ignition, Flame and Detonation in Gases* (Akad. Nauk SSSR, Moscow, 1960) [in Russian].
2. D. Downs, J. S. Street, and R. W. Wheeler, Fuel **32**, 279 (1953).
3. S. M. Sarathy, C. K. Westbrook, M. Mehl, et al., Combust. Flame **158**, 2338 (2011).
4. C. K. Westbrook, J. Warnatz, and W. J. Pitz, in *Proceedings of the 22nd International Symposium on Combustion* (Combust. Inst., Pittsburgh, 1988), p. 893.
5. H. Machrafi and S. Cavadias, Combust. Flame **155**, 557 (2008).
6. V. Ya. Basevich, A. A. Belyaev, V. S. Posvyanskii, and S. M. Frolov, Russ. J. Phys. Chem. B **7**, 161 (2013).
7. V. Ya. Basevich, A. A. Belyaev, and S. M. Frolov, Russ. J. Phys. Chem. B **9**, 268 (2015).
8. V. Ya. Basevich, A. A. Belyaev, S. N. Medvedev, V. S. Posvyanskii, and S. M. Frolov, Russ. J. Phys. Chem. B **9**, 933 (2015).
9. V. Ya. Basevich, A. A. Belyaev, S. N. Medvedev, V. S. Posvyanskii, and S. M. Frolov, Russ. J. Phys. Chem. B **10**, 801 (2016).
10. S. S. Sergeev, S. M. Frolov, and B. Basara, Gorenie Vzryv **10** (2), 26 (2017).
11. R. C. Reid, J. Prausnitz, and T. Sherwood, *The Properties of Gases and Liquids* (McGraw-Hill, New York, 1966; Khimiya, Leningrad, 1982).

12. V. V. Azatyan, A. M. Kogan, M. G. Neigauz, A. I. Poroikova, and E. N. Aleksandrov, Kinet. Katal. **16**, 577 (1975).
13. CHEMKIN-PRO Release 15083, 2009. http://www.advanceduninstaller.com/CHEMKIN-PRO-Release-15083-0cb0c8b7ec35efaa87b700db705a6e1d-application.htm.
14. A. A. Belyaev and V. S. Posvyanskii, Inform. Byull. Gos. Fonda Algoritm. Programm SSSR, No. 3, 35 (1985).
15. A. C. Egerton, N. P. W. Moore, and W. T. Lyn, Nature (London, U.K.) **167**, 191 (1951).
16. A. G. Gaydon, N. P. W. Moore, and J. P. Simonson, Proc. R. Soc., Ser. A **230**, 1 (1955).
17. Y. Ohta and M. Furutani, Arch. Combust. **11**, 43 (1991).
18. D. L. Dietrich, in *Proceedings of the AIAA Aerospace Sciences Meeting, Orlando, FL,* 2010. doi: 102514/6.2010-1110
19. T. Farouk and D. L. Dietrich, Combust. Theory Model. **15** (4), 87 (2011).
20. V. Nayagam, D. L. Dietrich, P. V. Ferkul, et al., Combust. Flame **159**, 3583 (2012).
21. S. M. Frolov, V. Ya. Basevich, and S. N. Medvedev, Dokl. Phys. Chem. **470**, 150 (2016).
22. V. Ya. Basevich, A. A. Belyaev, S. N. Medvedev, V. S. Posvyanskii, F. S. Frolov, and S. M. Frolov, Russ. J. Phys. Chem. B **4**, 995 (2010).
23. V. Ya. Basevich, A. A. Belyaev, V. S. Posvyanskii, and S. M. Frolov, Russ. J. Phys. Chem. B **4**, 985 (2010).
24. V. Ya. Basevich, S. N. Medvedev, S. M. Frolov, F. S. Frolov, B. Basara, and P. Prishing, Gorenie Vzryv **9** (3), 36 (2016).
25. S. M. Frolov, V. Ya. Basevich, S. N. Medvedev, and F. S. Frolov, Russ. J. Phys. Chem. B **12**, 245 (2018).

Translated by M. Timoshinina